BULLETIN OF THE POLISH ACADEMY OF SCIENCES
TECHNICAL SCIENCES, Vol. 59, No. 3, 2011
DOI: 10.2478/v10175-011-0041-y

Model of the two well potential for Hg-atoms in the $Hg_{1-x}Cd_xTe$ alloy lattice

J. POLIT*

Institute of Physics, University of Rzeszów, 16A Rejtana St., 35-310 Rzeszów, Poland

Abstract. The problem of the additional phonon modes (APM) of the far infrared spectra in the range of 100–115 cm^{-1} for the $Hg_{1-x}Cd_xTe$ alloys has been discussed for the last forty years. The model of two well potential of the mercury atoms in the $Hg_{1-x}Cd_xTe$ lattice is proposed for interpretation of these APM. Analysis was performed for samples of different compositions ($0.06 < x < 0.7$) and different types (n- and p-type) of conductivity.

Key words: well potential, Hg-atoms, $Hg_{1-x}Cd_xTe$ alloy lattice.

1. Introduction

The $Hg_{1-x}Cd_xTe$ system is unique because its band structure can be modified from an inverted band structure with the negative energy gap $E_g = -0.3$ eV (for HgTe) to the "normal" band structure with the energy gap equal to about $E_g = 1.4$ eV (for CdTe) and the lattice mismatch between compounds above mentioned is lattice is practically zero. The HgCdTe is main material for IR detectors [1–4].

According the EXAFS measurements [5] the nearest – neighbor bond lengths in the $Hg_{1-x}Cd_xTe$ crystals are found to be constant as a function of alloy compositions within experimental uncertainties 0.01 A. It means that substitution of the Hg-cation by a Cd-cation does not cause lattice deformations. On the other hand, the week Hg-Te bond (introducing of Cd-atoms to the lattice weaken this bond more in $Hg_{1-x}Cd_xTe$ [6]) causes such self-defects as Hg-vacancy to be thermodynamically stable in the Hg-sublattice [7]. The problem of Hg-vacancies in the lattice is also discussed in papers dedicated to phonon spectra of MCT [8–12].

It is known that the far-infrared (FIR) spectra gives a direct information about phonon modes in the crystal lattices as well as about impurity levels. Infrared spectroscopy also enables us also to obtain information about real local crystalline structure and interactions occurring in the system [8]. If the intrinsic point defects or impurity defects, are present in the ideal tetrahedron structure, additional frequencies, related to the specific properties of each defect appear in the optical spectra. Indeed, all such defects deform the structural unit of the lattice – in the case of the tetrahedron coordination structure (zincblende and wurtzite) it is an ideal elemental tetrahedron described as a cation/anion at the centre of a tetrahedron with four anions/cations at its vertexes. The size of the tetrahedron deformation depends on the kind of the defects. Actually, the tetrahedron deformation modifies the electron charge distribution within the tetrahedron and consequently affects the distribution of the potential and of the field around all the constituents. The perturbation to the force field is responsible for the change in the vibrational spectra, with the appearance of new or modified frequencies due to local or resonant vibrational modes [8–10]. An additional mode caused by introducing of the hydrogen atoms in the tetrahedra in the crystal lattice of CdTe was observed in the FIR-spectra obtained using synchrotron radiation as the source [11]. The problem of the additional phonon modes (APM) in the 100–115 cm^{-1} range has existed for the $Hg_{1-x}Cd_xTe$ alloys for the last forty years [13–22]. The additional mode is observed too in HgTe crystals in this same range [23, 24]. One of subjects concerning the phonon spectra of alloys is the percolation model of the vibrational properties of the solid solutions, developed in years 2002–2008 by Pages with co-authors and described in the work [25].

The most comprehensive experimental investigation of the $Hg_{1-x}Cd_xTe$ phonon spectra was undertaken by Kozyrev et al. [17], where the composition dependence of the subtle structure of two sub-bands HgTe-like and CdTe-like were observed and analysed in detail and an interpretation in terms of five based cells (tetrahedra) was presented. Nevertheless, the region below 118 cm^{-1} was excluded from consideration in [17]. However, several experiments have indicated that in the range of about 100–115 cm^{-1} additional lines are located [12–18]. There are important guiding principles that these lines are related to the defects [11, 12, 18–20]. In our earlier short communication [16] was shown that the spectral lines at 100–115 cm^{-1} can be related to the Hg-vacancies. This interpretation was changed in our next work [12]. This paper is concentrates on the structural problem of two valley potential positions of Hg-atoms in the $Hg_{1-x}Cd_xTe$ lattice. The data from the FIR spectra are used for justification of this new conception.

*e-mail: polijack@univ.rzeszow.pl

2. Theory. Model of the two well potential for Hg-atoms in the lattice

On the basis of the Sussman [26] theory we consider two single well with the wave functions ψ_1 and ψ_2^0 which differ only by the fact of being centered at different minima of the double potential well. They overlap in general and we define the overlap integral:

$$\int_{-\infty}^{+\infty} \psi_1^0 \psi_2^0 dx = \Delta. \tag{1}$$

The wave function ψ_1 has to be orthonalized. Assuming small values of Δ we keep only the first term of his general expression. Following Sussman we get the expressions for wave functions

$$\begin{aligned} \psi_1^I &= \left(1 + \frac{3\Delta^2}{8}\right)\left(\psi_1^0 - \frac{\Delta}{2}\psi_2^0\right), \\ \psi_2^I &= \left(1 + \frac{3\Delta^2}{8}\right)\left(\psi_2^0 - \frac{\Delta}{2}\psi_1^0\right) \end{aligned} \tag{2}$$

and for Hamiltonians

$$\begin{aligned} H_{11}^I = H_{22}^I &= \left(1 + \frac{3\Delta^2}{4}\right)\left|H_{11}^0\left(1 - \frac{\Delta^2}{4}\right) - \Delta H_{12}^0\right|, \\ H_{12}^I = H_{21}^I &= \left(1 + \frac{3\Delta^2}{4}\right)\left|H_{12}^0\left(1 - \frac{\Delta^2}{4}\right) - \Delta H_{11}^0\right|. \end{aligned} \tag{3}$$

An asymmetric potential U which can be split into symmetrical and antisymetrical components U_s and U_a (relative to the middle point between the potential wells) is superposed on the symmetrical double potential well.

The Hamiltonian matrix $H^I + U^I$ can be diagonized with a transformation matrix T

$$T = \begin{vmatrix} \cos\frac{\varphi}{2} & \sin\frac{\varphi}{2} \\ -\sin\frac{\varphi}{2} & \cos\frac{\varphi}{2} \end{vmatrix} \tag{4}$$

with

$$\tan\varphi = \frac{H_{12}^I + U_{s12}^I}{U_{a,11}^I}. \tag{5}$$

Leading to the energies ($U_{a,12}^I$ being identically zero):

$$H_{11}^I + U_{s,11}^I \pm [(H_{12}^I + U_{s,12}^I)^2 + (H_{s,11}^I)^2]^{1/2}. \tag{6}$$

An alternative definition of the degree of localization of the resulting wave function can be taken as $T_{21}^2/T_{11}^2 = T_{12}^2/T_{22}^2 = \tan^2\varphi/2$. Within the limit $\Delta \to 0$, this definitions coincides with the previous one. All definitions are arbitrary to a certain degree. A physically meaningful definition can only be given if the measuring process is specified. For small values of ϕ and Δ however, the discrepancies will be negligible.

The superimposed potential will now be further decomposed in a static and a time dependent part. U_o designates the static part . Physically the static part will be responsible for the localization of the states in one or the other well, whereas the time dependent part will be responsible for transition between these localized stationary states. Introducing only the static part U_o into the transformating matrix T we are left with off-diagonal where U_{ta} is the antisymmetrical U_{ts} the symmetrical part of the time dependent perturbation potential.

For strong localization we may write

$$\begin{aligned} \cos\varphi &\cong 1, \\ \sin\varphi &= \frac{H_{12}^I + U_{0a,12}^I}{U_{0a,11}}. \end{aligned} \tag{7}$$

As mentioned above, the static part U_0 originates from internal strain self polarization or externally applied fields. As for the time dependent part U_t will consist of superpositions of oscillatory terms. To each phonon mode σ corresponds a term u_σ. Its form will depend on how the system under consideration is coupled to the surrounding host lattice. Some possibilities are described below.

1. The local strain changes the barrier height giving a symmetrical contribution $u_{\sigma s}$ which is a functional of the local strain.
2. The local strain changes the distances between the potential wells. This can again be described as additional symmetrical potential $u_{\sigma s}$ which contains linear and higher power terms in the local strain.
3. The local strain produces an energy differences between the two localizations giving an antisymmetric contribution.
4. The whole system is rigidly displayed by the elastic wave. Only quadratic and higher order terms appear.

Once the coupling mechanism is given, the transitions probabilities can be calculated along the same line. The displacement ΔR of the point R is given by:

$$\Delta R = \sum_\sigma V_a \left(\frac{\hbar}{2\rho V \nu_\sigma}\right)^{1/2} (a_\sigma \exp(ik_\sigma R) + a_\sigma^* \exp(ik_\sigma R)), \tag{8}$$

where σ designates the phonon mode of propagation vector k_σ and polarization vector $\hat{\upsilon}_\sigma$ and frequency ν_σ and c is the sound velocity ρ is the density of the crystal and V its volume; and a a* are phonon absorption and emission operators.

Sussman [26] proposed this model for the binary compounds. According to his theory a cation in the crystal lattice could have the two positions: first a stable position energetically more deep, the second is a metastable state with higher energy and corresponding to a longer Hg-Te bond than that in the previous case This model related to HgTe and $Hg_{1-x}Cd_xTe$ means that the Hg atoms can be shifted from the vertex position in the tetrahedra (stable position) to a non centered position (metastable position).

According to Sussman's theory such a transition from stable to metastable state, means that the Hg-Te bonds become longer. The probability for such transition is described by

$$W = w \exp(-\Delta E/kT), \tag{9}$$

where ΔE is the energy difference between the two states – stable and metastable one (see Fig. 1) and w is the assumed probability at the absolute zero.

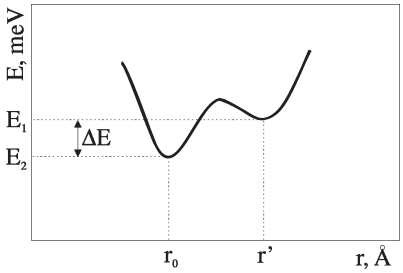

Fig. 1. Model of the two wells potential for Hg-atoms

3. Description of Experiment

3.1. Samples and experimental procedure. The nine $Hg_{1-x}Cd_xTe$ samples were being examined ($x = 0.06 - 0.7$) were obtained by the liquid phase epitaxy method (LPE). Special attention was given to samples with a comparable identical $x = 0.2$ composition, but with different types of conductivity. In the case of the n-type with concentration obtained from measurements of the Hall effect at temperature 77 K is equal to 6.5×10^{13} cm^{-3} and in the case of p-type concentration $p = 3.5 \times 10^{15}$ cm^{-3}. It should be emphasized that electron mobility in the n-type sample was very high $\mu = 2.3 \times 10^5$ cm^2/V s at 77 K [27–29]. FIR reflectivity experiments were performed at the DAΦNE – light laboratory at Frascati (Italy) using the experimental set-up described in [30]. We used a BRUKER Equinox 55 FT-IR interferometer modified to collect the spectra in a vacuum. We used as IR sources both the synchrotron radiation from the DAΦNE storage ring and a mercury lamp. Measurements were taken over a temperature range of 20–300 K and for frequencies ranging from 50 to 600 cm^{-1}. In order to provide the spectral resolution of 1 cm^{-1} (2 cm^{-1} in some case) we typically collected 200 scans within 600 s of acquisition time with a bolometer cooled to 4.2 K.The reflectivity was measured using as reference a gold film evaporated onto the surface of the samples investigated. This method enabled us to measure the reflectivity coefficient with an accuracy of about 0.2%.

3.2. The curves of the imaginares part of the dielectric function. The optical reflection of the samples mentioned above were measured. Usually the curves Im$[\varepsilon(\omega, T)]$ imaginary part of the dielectric function extracted from the reflection spectra by the Kramers-Kroning transformation are interpreted. The curves of the imaginary part of the dielectric function Im$[\varepsilon(\omega, T)]$ for the measured samples of different compositions are presented in Figs. 2–5.

Three bands are clearly seen in Fig. 2 for the sample $Hg_{0.94}Cd_{0.06}Te$: the first around 95–115 cm^{-1} the second at 115–130 cm^{-1} with a higher amplitude and a third band around 140–160 cm^{-1} with a lower amplitude. As was mentioned in the introduction the band at 95–115 cm^{-1} is caused by APMs while the others two bands are caused by so called canonical phonon modes (CPM) which will be explained in Sec. 4. In Fig. 3 the imaginary part of the dielectric function for $Hg_{0.72}Cd_{0.28}Te$ is presented. It is seen three bands too for the sample $Hg_{0.72}Cd_{0.28}Te$ one around 95–115 cm^{-1} with comparable amplitude to sample $Hg_{0.94}Cd_{0.06}Te$ second 115–130 cm^{-1} with smaller amplitude in comparison to Fig. 2 and a third band around 140–160 cm^{-1} with higher amplitude in comparison to the sample $Hg_{0.94}Cd_{0.06}Te$.

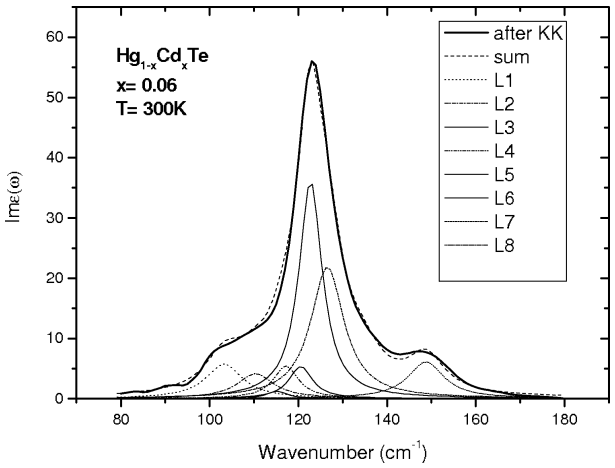

Fig. 2. Spectral analysis of the phonon bands of $Hg_{0.94}Cd_{0.06}Te$ at temperature 300 K, L1-L8 Loretzians whose parameters are described in Table 1

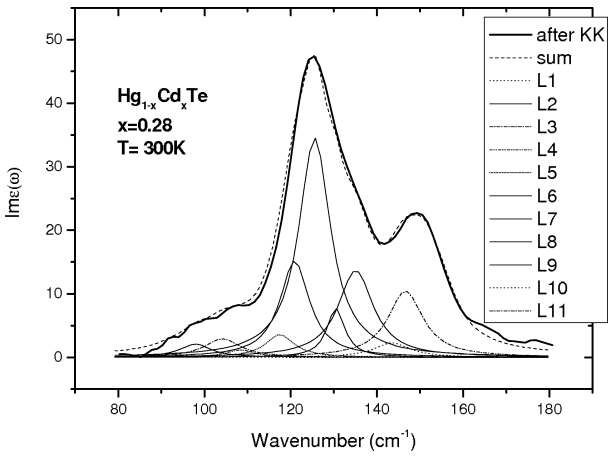

Fig. 3. Spectral analysis of the phonon bands of $Hg_{0.72}Cd_{0.28}Te$ at temperature 300 K, L1-L11 Loretzians whose parameters are described in Table 2

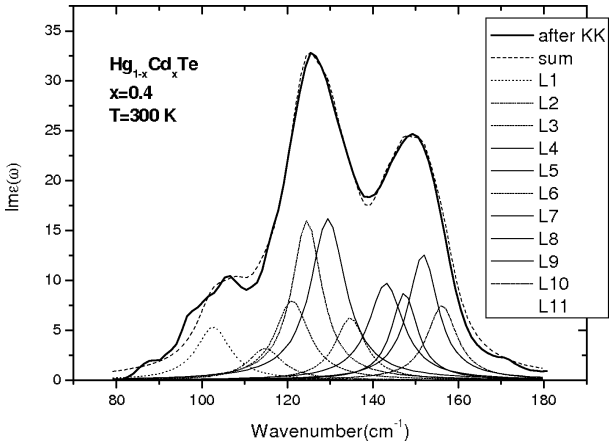

Fig. 4. Spectral analysis of the phonon bands of $Hg_{0.6}Cd_{0.4}Te$ at temperature 300 K, L1-L11 Loretzians whose parameters are described in Table 3

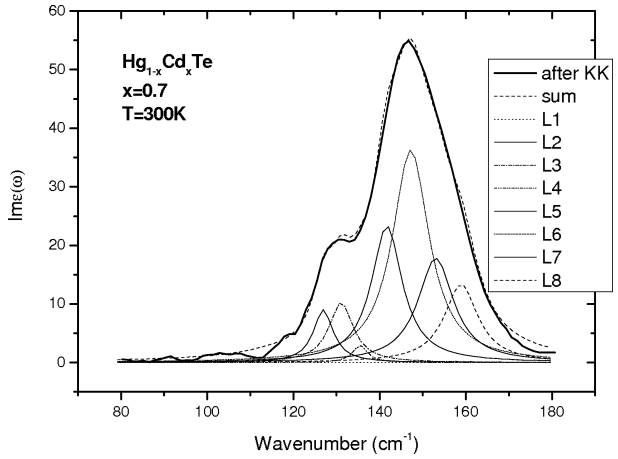

Fig. 5. Spectral analysis of the phonon bands of $Hg_{0.3}Cd_{0.7}Te$ at temperature 300 K, L1-L8 Loretzians whose parameters are described in Table 4

In Fig. 4 the imaginary part of the dielectric function for $Hg_{0.6}Cd_{0.4}Te$ is presented.

Three bands can be seen one around 95–115 cm^{-1} with comparable amplitude to samples $Hg_{0.72}Cd_{0.28}Te$ second 115–130 cm^{-1} with smaller amplitude in comparison to Fig. 3 and third band around 140–160 cm^{-1} with higher amplitude in comparison to sample $Hg_{0.72}Cd_{0.28}Te$, (see Fig. 3).

In Fig. 5 the imaginary part of the dielectric function for $Hg_{0.3}Cd_{0.7}Te$ is presented also three bands can be seen: one around 95–115 cm^{-1} with smaller amplitude in comparison to the sample in Fig. 2, 3 and 4, the second band 115–130 cm^{-1} with a smaller amplitude in comparison to Fig. 4 and the third band around 140–160 cm^{-1} with a higher amplitude in comparison to the sample $Hg_{0.6}Cd_{0.4}Te$.

4. Analysis of the phonon bands of $Hg_{1-x}Cd_xTe$

4.1. General notes. In the case of a solid solution FIR spectra the imaginary part of the dielectric function may be approximated as the sum of Lorentzians describing the k-phonon modes:

$$\mathrm{Im}\varepsilon(\omega) = \sum_{i=1}^{k} \frac{S_i \gamma_i \omega}{(\omega_{TOi}^2 - \omega^2)^2 + \omega^2 \gamma_i^2}, \qquad (10)$$

where S_i, ω_{TOi} and γ_i are the oscillator strength, frequency and damping parameter of the i-phonon mode, respectively.

According to the Verleur-Becker (V-B) model [31] the crystalline lattice of the $A_{1-x}B_xZ$ C alloy consisted of five structural units: In zincblende (ZB) or ternary compounds the model proposed by (V-B) is based on *five* basic elemental tetrahedra with a Z anion at the centre and *four* A cations at the vertexes. An alternative model (strained tetrahedron model) has been proposed in [8] $\{T_k\}_{k=0.4}$, with two binary T_0: A^4Z, T_4: B^4Z, and three ternary $T_{k=1,2,3}$: A^3B^1Z, A^2B^2Z, A^1B^3Z, the subscript k indicating the number of B atoms in the Z-centered tetrahedron, while (4-k) is the number of A ions. In zincblende ternary $A_{1x}B_xZ$ (or AY_yZ_{1y}) compounds, each vibrating ion dipole-pair AZ and BZ, from each of the five elemental tetrahedron configurations $\{T_k\}_{k=0.4}$ contributes with a phonon line to an IR spectrum.

For HgCdTe ideal lattices four HgTe-like CPMs and four CdTe-like contribute to the sum in the Eq. (1). Within this approximation the experimental Im$[\varepsilon(\omega, T)]$-curves, allow one to find the S_i values.

4.2. Analysis of phonon spectra for different compositions. The dispersion analysis of the main phonon bands was performed by approximating the Im$[\varepsilon(\omega, T)]$ curves by the Lorentzian sum (Eq. (10)). The results of spectral analysis for sample $Hg_{1-x}Cd_xTe$, ($x = 0.06$ to $x = 0.7$) are presented in Figs. 2–4, 6, 7 and Table 1–4.

The parameters of Lorentzian's oscillators are presented in Table 1 for sample $Hg_{0.94}Cd_{0.06}Te$.

The curve of the imaginary part of the dielectic function Im$[\varepsilon(\omega)]$ – for sample $Hg_{0.94}Cd_{0.06}Te$ is approximated using eight Lorentzians: three Lorentzians belonging to additional phonon modes (APM) and five to canonical phonon modes (CPM). The Lorentzians amplitude APM are comparable with amplitude of CPM for the CdTe sublattice.

The parameters of Lorentzian's oscillators for the n-$Hg_{0.72}Cd_{0.28}Te$ are presented in Table 2.

The imaginary part of the dielectic function Im$[\varepsilon(\omega)]$ – for sample $Hg_{0.72}Cd_{0.28}Te$ is a possible approximation with the help of eleven Lorentzians, seven Lorentzians belonging to canonical phonon modes (CPM) and four to additional phonon modes(APM), see Figs. 3 and 4. The amplitude of APM have the small amplitude in comparison to CPM. Parameters of Lorentzian's oscillators for the $Hg_{0.6}Cd_{0.4}Te$ for the temperatures 300 K are presented in Table 3.

Table 1
Parameters of Lorentzian's oscillators used for fitting the Im$[\varepsilon(\omega, T)]$ – curves of the $Hg_{0.94}Cd_{0.06}Te$ for temperatures 300 K

Temperature [K]	Number of line	S (cm^{-2})	ω (cm^{-1})	γ (cm^{-1})	$\sum S_{HgTe}$ CPM	$\sum S_{HgTe}$ APM	$\sum S_{CdTe}$ CPM	$\sum S_{CdTe}$ APM	S/ω^2
300	1	6000	104.0	10	60200	11500			0.554
	2	4700	111.0	7.8					0.381
	3	800	115.7	5.5					0.059
	4	5200	117.2	5.6					0.378
	5	13000	121.0	6.3					0.887
	6	26000	123.2	6.3					1.712
	7	16000	129.0	7.0					0.961
	8	8900	149.0	9.5			8900		0.400

Table 2
Parameters of Lorentzian's oscillators used for fitting the $\mathrm{Im}[\varepsilon(\omega,T)]$ – curves of the $Hg_{0.72}Cd_{0.28}Te$ for the temperatures 300 K

Temperature [K]	Number of line	S (cm^{-2})	ω (cm^{-1})	γ (cm^{-1})	$\sum S_{HgTe}$ CPM	$\sum S_{HgTe}$ APM	$\sum S_{CdTe}$ CPM	$\sum S_{CdTe}$ APM	S/ω^2
300	1	3400	103.7	9.4	59090	5160	34900		0.316
	2	870	110.0	10.0					0.071
	3	890	115.5	9.5					0.066
	4	27200	121.5	9.5					1.842
	5	17000	125.0	6.5					1.088
	6	14000	129.0	6.3					0.841
	7	800	131.0	6.0					0.046
	8	23000	135.0	10.0					1.262
	9	15300	146.70	10.0					0.710
	10	12800	150.5	7.6					0.565
	11	6800	155.7	6.6					0.280

Table 3
Parameters of Lorentzian's oscillators used for fitting the $\mathrm{Im}[\varepsilon(\omega,T)]$ – curves of the $Hg_{0.6}Cd_{0.4}Te$ for the temperatures 300 K

Temperature [K]	Number of line	S (cm^{-2})	ω (cm^{-1})	γ (cm^{-1})	$\sum S_{HgTe}$ CPM	$\sum S_{HgTe}$ APM	$\sum S_{CdTe}$ CPM	$\sum S_{CdTe}$ APM	S/ω^2
300	1	5200	103.5	9.4	46440	12110	48440		0.485
	2	3410	108.7	8.5					0.288
	3	3500	115.5	9.5					0.262
	4	9240	121.7	9.5					0.623
	5	16600	125.1	8.3					1.060
	6	20600	130.0	9.8					1.21
	7	7100	135.1	8.4					0.388
	8	13500	143.4	9.7					0.656
	9	9300	147.6	7.2					0.426
	10	15900	151.9	8.2					0.689
	11	9740	156.3	8.3					0.398

Table 4
Parameters of Lorentzian's oscillators used for fitting the *Im[εοωsTp]g*−curves of the $Hg_{0.3}Cd_{0.7}Te$ for the temperatures 300 K

Temperature [K]	Number of line	S (cm^{-2})	ω (cm^{-1})	γ (cm^{-1})	$\sum S_{HgTe}$ CPM	$\sum S_{HgTe}$ APM	$\sum S_{CdTe}$ CPM	$\sum S_{CdTe}$ APM	S/ω^2
300	1	300	114.4	9.0	15300	300	129900		0.022
	2	6300	127.4	5.5					0.388
	3	9000	131.5	6.7					0.520
	4	1600	135.8	4.0					
	5	28400	142.0	8.6					1.408
	6	54600	147.5	10.2					2.509
	7	27000	153.2	9.9					1.150
	8	19900	159.0	9.4					0.787

The imaginary part of the dielectric function $\mathrm{Im}[\varepsilon(\omega)]$ – for sample $Hg_{0.6}Cd_{0.4}Te$ is a possible approximation with the help of eleven Lorentzians, four Lorentzians belonging to additional phonon modes (APM) and seven (three Lorentzians belonging to HgTe-like and four Lorentzians belonging to CdTe-like mode) to canonical phonon modes(CPM), see Fig. 3 and Fig. 6. The amplitude of APM is large in comparison to sample $Hg_{0.72}Cd_{0.28}Te$.

Parameters of Lorentzian's oscillators for $Hg_{0.3}Cd_{0.7}Te$ are presented in Table 4.

The composition dependencies of the phonon mode dependencies for $Hg_{1-x}Cd_xTe$ at 300 K, is presented in Fig. 6.

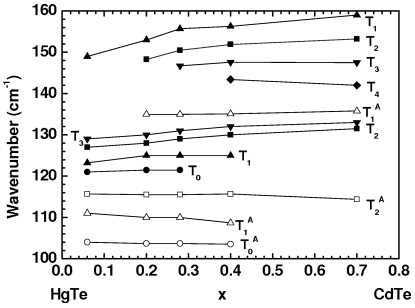

Fig. 6. The composition dependencies of the phonon mode dependencies for $Hg_{1-x}Cd_xTe$ at 300 K. The open symbols T_o^A, T_1^A, T_2^A – described tetrahedra generated additional phonon mode containing Hg – atoms in metastable positions

The imaginary part of dielectic function Im$[\varepsilon(\omega)]$ – for sample $Hg_{0.3}Cd_{0.7}Te$ is a possible approximation with the help of eight Lorentzians, two Lorentzians belonging to additional phonon modes (APM) and six (two Lorentzians belongin to HgTe-like and four Lorentzians belonging to CdTe-like mode) to canonical phonon modes(CPM), see Fig. 4 and Fig. 6. The amplitude of APM is smaller in comparison to previous sample.

4.3. Analysis of phonon spectra for different temperature and type of conductivity. The parameters of Lorentzian's oscillators used for fitting curves of the Im$[\varepsilon(\omega, T)]$ are shown in Table 5 for the sample n-type $Cd_{0.2}Hg_{0.8}Te$ at the temperatures 30 K and 300 K and in Table 7 for the p-$Cd_{0.2}Hg_{0.8}Te$ one. It is seen from Fig. 8a that the curve of the Im$[\varepsilon(\omega, T)]$ for n-$Cd_{0.2}Hg_{0.8}Te$ at 30 K may be approximated by the sum of the four Lorentzian's oscillators only. When the temperature increases the observed two sub-bands of the Im$[\varepsilon(\omega, T)]$ are considerably wider (see Fig. 9a) and the number of the Lorentzins necessary for approximation, increases to nine.

The analogous dissipation of the Im$[\varepsilon(\omega, T)]$ curves on the Lorentzians was carried out for the p-type $Cd_{0.2}Hg_{0.8}Te$ sample (see Fig. 7b and 8b). The parameters of these oscillators are presented in Table 7.

There are nine well-resolved oscillators for p-type $Hg_{0.8}Cd_{0.2}Te$ at 30 K and eleven for this sample at 300 K. The positions of the main HgTe-lines for n- and p-type are the same (118 cm^{-1}) at 30 K while the oscillator strengths of these two lines are drastically different: 62500 cm^{-2} for the n-type and 39000 cm^{-2} for the p-type, correspondingly, the damping factor is nearly two times larger for the p-type because the line shape is much more asymmetric and wider for the p-type $Hg_{0.8}Cd_{0.2}Te$. Additionally, the level of the background for the p-type $Hg_{0.8}Cd_{0.2}Te$ on the left side is essentially higher than for the n-type $Hg_{0.8}Cd_{0.2}Te$.

Table 5
Parameters of Lorentzian's oscillators used for fitting curves of the for the $Cd_{0.2}Hg_{0.8}Te$ sample n-type for the temperature range 30 K $-$300 K

Temperature [K]	Number of line	S (cm^{-2})	ω (cm^{-1})	γ (cm^{-1})	$\sum S_{HgTe}$ CPM	$\sum S_{HgTe}$ APM	$\sum S_{CdTe}$ CPM	$\sum S_{CdTe}$ APM
30	1	500	107.0	6.4		500		
	2	62500	118.0	1.35	62500			
	3	8400	151.0	7.7			19900	
	4	11500	153.7	8.4				
300	1	500	103.0	5.0		5100		
	2	3000	115.0	8.0				
	3	1600	118.7	4.0	37200			
	4	30800	122.6	2.8				
	5	3000	125.0	5.0				
	6	3500	128.6	5.0				
	7	1600	135.0	7.0				1600
	8	4000	147.3	4.7			9400	
	9	5400	151.5	6.3				

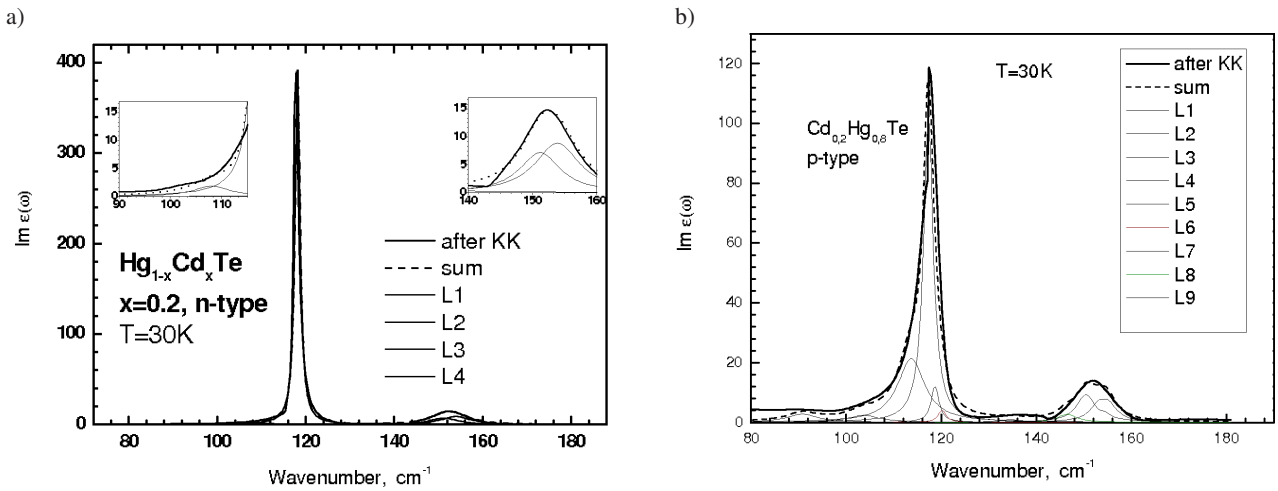

Fig. 7. Spectral analysis of the phonon bands of $Cd_{0.2}Hg_{0.8}Te$ n-type (a) and p-type (b) at temperature 30 K

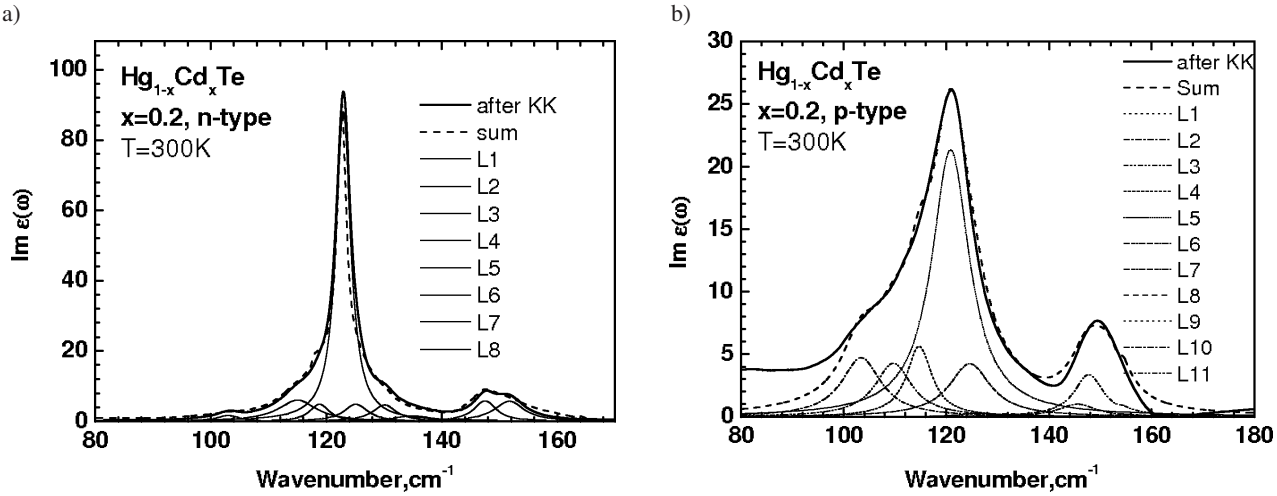

Fig. 8. Spectral analysis of the phonon bands for n-type $Hg_{0.8}Cd_{0.2}Te$ (a) and p-type $Hg_{0.8}Cd_{0.2}Te$ (b) at temperature 300 K. L1-L11 are the Lorentzians whose parameters are presented in Table 7

Table 6
The specific oscillator's strength sums of the CPM and APM for n-$Hg_{0.8}Cd_{0.2}Te$ at 30 K and 300 K

Temperature [K]	$s^i_{\mathrm{HgTe}} = \dfrac{S^i_{\mathrm{HgTe}}}{\omega^2}$	$\left(\sum_j s^j_{\mathrm{HgTe}}\right)_{add}$
30	4.49	0.043
300	2.45	0.37

Table 7
Parameters of Lorentz oscillators used for fitting curves of the Kramersa Kroniga transformation for the $Cd_{0.2}Hg_{0.8}Te$ sample p-type for the temperature range 30–300 K

Temperature [K]	Number of line	S (cm^{-2})	ω (cm^{-1})	γ (cm^{-1})	$\sum S_{\mathrm{HgTe}}$		$\sum S_{\mathrm{CdTe}}$	
					CPM	APM	CPM	APM
30	1	600	91.00	5.0		6200		
	2	1500	107.0	4.0				
	3	4700	112.4	4.0				
	4	48000	118.0	3.5	48000			
	5	500	135.0	7.0				500
	6	1300	148.0	5.0				
	7	5800	151.0	5.0			15800	
	8	8700	154.2	6.2				
300	1	4200	103.7	8.6		11400		
	2	4200	110.0	8.1				
	3	6100	115.0	7.7				
	4	21100	121.3	7.7				
	5	830	125.0	7.0	31300			
	6	1000	127.0	7.0				
	8	1200	135.0	7.0				1000
	9	1300	146.1	8.9				
	10	3500	148.3	7.0			9690	
	11	4890	152.0	7.4				

Table 8
The oscillator's sums of the CPM and APM for p-$Hg_{0.8}Cd_{0.2}Te$ at 30 K and 300 K

Temperature [K]	$s^i_{\mathrm{HgTe}} = \dfrac{S^i_{\mathrm{HgTe}}}{\omega^2}$	$\left(\sum_j s^j_{\mathrm{HgTe}}\right)_{add}$
30	2.8	0.5
300	1.54	1.19

When the temperature increased to 300 K the differences between the n- and p-type of $Hg_{0.8}Cd_{0.2}Te$ decreases: the oscillator strengths of the main lines are 30800 cm^{-2} and 21000 cm^{-2}, respectively, the number of the Lorentzins increases to nine and eleven for n- and p-type HgTe-like sub-bands, respectively. We observed several additional lines in the range 90 cm^{-1} to 115 cm^{-1} for the p-type $Hg_{0.8}Cd_{0.2}Te$ at 30 K.

5. Interpratation of the experimental results

It is interesting to consider in details the temperature behavior of the phonon modes observed for both the n- and p-type $Hg_{0.8}Cd_{0.2}Te$. In Figs. 7 and 8 are shown the temperature dependences of frequencies for the phonon lines of HgTe-like and CdTe-like sub-bands of n- and p-type samples are shown. It is seen that only one HgTe-like mode is observed at 30 K and two CdTe-like modes for n-$Hg_{0.8}Cd_{0.2}Te$. When the temperature is higher than 100 K the splitting on two HgTe-like modes takes place and finally at 300 K the three HgTe-like phonon modes are displayed in the case of the n-type sample. The weak line is observed at 108 cm^{-1} whose amplitude increases with increasing of temperature and after 230 K this line is split into three in the range 118–103 cm^{-1}.

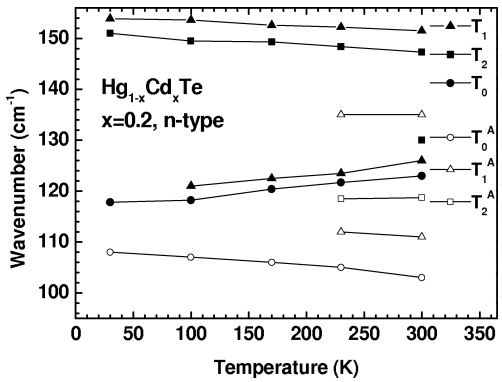

Fig. 9. The temperature dependencies of the phonon mode frequencies for n-$Hg_{0.8}Cd_{0.2}Te$ shown in Fig. 8a and Table 5. T_0, T_1 and T_2 are tetrahedra generated the corresponding CPM modes. T_n^A are tetrahedra generated by the corresponding APM modes

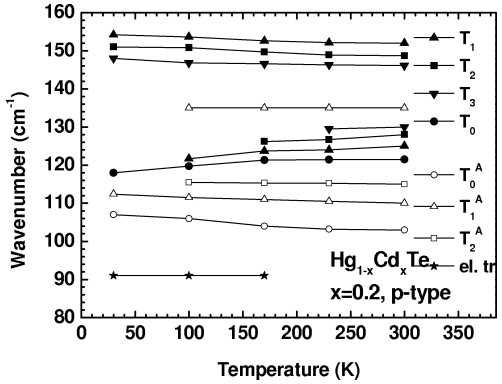

Fig. 10. The temperature dependencies of the phonon mode frequencies for the $p-$ type $Hg_{0.8}Cd_{0.2}Te$, shown in Fig. 8b and 9b. T_0, T_1 and T_2 are tetrahedra generated the corresponding CPM modes. T_n^A are tetrahedra generated by the corresponding APM modes, el.tr – electron transition

The temperature dependencies of the phonon mode frequencies for p-$Hg_{0.8}Cd_{0.2}Te$ are presented in Fig. 10. We can see a considerably larger number of lines here in comparison to the n-type sample but the temperature shift of the phonon mode frequencies is similar.

6. Temperature dependencies of the specific oscillator strength sum

As was mentioned in the introduction, there are important guiding principles that the lines in the region 104–116 cm^{-1} are related to the Hg-vacancies. This hypothesis can be verified by temperature dependences of the specific oscillator strength sum (SOSS) of the lines observed in this region. These temperature dependences are presented in Fig. 11 for p-$Hg_{0.8}Cd_{0.2}Te$ Te upper curve and in Fig. 11 lower curve for n-$Hg_{0.8}Cd_{0.2}Te$.

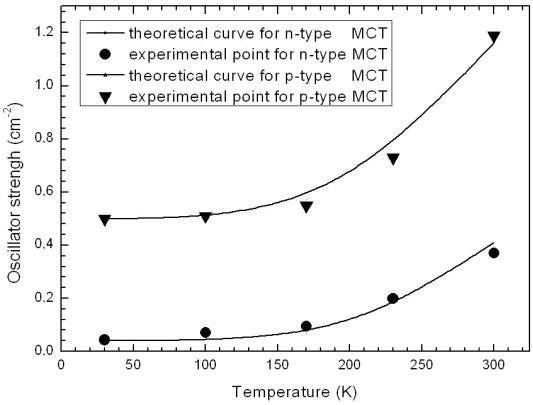

Fig. 11. The temperature dependence of the sum of the additional modes oscillator strengths for the n-type $Hg_{0.8}Cd_{0.2}Te$, circle- experimental points, the continuous line is an approximated curve calculated according the equation $s = 0.04+12\exp(-0,09/kT)$.The upper curve is the temperature dependence of the sum of the additional modes oscillator strengths for the p-type $Hg_{0.8}Cd_{0.2}Te$, triangle-experimental points, the continous line is the approximated curve calculated according the equation $s = 0.5 + 12\exp(-0.075/kT)$

It is shows in Fig. 11 that temperature dependency of the SOSS of APMs for p-type $Hg_{0.8}Cd_{0.2}Te$, have the exponential character described by the function

$$\sum s_{\mathrm{HgTe}}^{add} = 0.5 + 12\exp(-0.075/kT) \qquad (11)$$

with activation energy equal to 75 meV. It is too small energy in comparison with the Hg-vacancy activation energy to be equal to about 1 eV [7].

The Fig. 11 presents the temperature dependency of the SOSS of the same lines for n-type $Hg_{0.8}Cd_{0.2}Te$. This dependency is described by the exponential function similar to (9):

$$\sum s_{\mathrm{HgTe}}^{add} = 0.04 + 12\exp(-0.09/kT) \qquad (12)$$

with activation energy equal to 90 meV, which is larger than for the p-type but too small to be an activation energy for Hg-vacancies.

It is clear that the temperature dependencies of the SOSS of the lines observed in the region of 104–116 cm^{-1} does not confirm the hypothesis that these lines are related to the Hg-vacancies. There are other doubtful circumstances, namely: in the case of the n-type $Hg_{0.8}Cd_{0.2}Te$ a single very weak line at 107 cm^{-1} is observed at 30 K also. If we assume that this line is caused by Hg- vacancies it is necessary to agree that the vacancy density must be not less than 10^{18} cm^{-3}. This is an absurdly large number of defects for a crystal with the electron mobility equal to 2.3×10^5 cm^2/V s. While the data of the positron annihilation for n-type $Hg_{1-x}Cd_xTe$ shown values of the Hg-vacancy concentration rather closer to 10^{15} cm^{-3} [32]. It is necessary to note that the method of the positron annihilation, seems to be a direct method of the vacancy concentration measurement, in the case of Hg CdTe using the data of the Hall-effect (in determination of the specific positron trapping rate) to identify the hole concentration to the concentration of Hg-vacancies ($p = C_V^{Hg}$ for the model p-type HgCdTe). This is not completely correct because in HgCdTe there is always background of the electrically native compensated Hg-vacancies and the real level of the Hg-vacancies is naturally higher than the hole concentration. Nevertheless, the Hg-vacancy density over 10^{18} cm^{-3} in the n-$Hg_{0.8}Cd_{0.2}Te$ Te of high quality (very high electron mobility) is absolutely impossible.

In the case of the p-type $Hg_{0.8}Cd_{0.2}Te$ the C_V^{Hg} is higher by about two or three orders of magnitude but it is difficult to assumed that it can achieve the value of 10^{21} cm^{-3} (about a few molar percent which means that the density of Hg-vacancies should be the same as the density of the matrix atoms) as seen from the spectra shown in Fig. 8b and 9b. This is also impossible.

Therefore, it is necessary to find a credible hypothesis which could explain the presence of lines in the range 104–116 $cm^{-1}$for HgTe and HgCdTe.

The temperature dependences of the SOSS for these lines lead us to the activation energy of the process to be equal to 75–90 meV which could be a substantial argument for applying the model of two potential wells for Hg-atoms in a lattice of HgCdTe).

The temperature dependences of SOSS for APM shown in Fig. 11 and described by relations 11 and 12 enable us to determine the ΔE. Therefore, in the case of the p-type $Hg_{0.8}Cd_{0.2}Te$ the energy transition from the stable position of the Hg atoms to the metastable position is 75 meV and 90 meV for the n-type one. This difference can be explained by the fact that for p-type material where the considerable path of the crystal lattice is non relaxed, the density of metastable state is larger than in the n-type which could change the depth of the energy minimum (value E_2) for the stable position. The ratio of the SOSSs of the additional lines (104–116 cm^{-1}) for p- and n-type materials is about one order. Therefore, the density of the metastable states and stable states should differ by the same value. Simultaneously, the length of the Hg-Te bonds is longer for the metastable states in comparison to the stable state This difference can be noticed in X-ray analyses.

7. X-ray structural analysis

The X-ray diffraction spectra performed at 300 K for n- and p-type $Hg_{0.8}Cd_{0.2}Te$ samples, as well as the far-infrared reflectivity spectra were investigated and shown in Fig. 12ab, demonstrate the essential differences in both position of the diffraction maxima as well as the shapes of these maxima. It is seen in Fig. 12a that maximum corresponding to 111 face have different position for n- and p-type materials, namely $2\theta = 23.811$ degree and $2\theta = 23.275$ degree, respectively. The lattice parameters derived from these positions are: 6.4648 Å and 6.4604 Å, respectively. It means that the lattice for the n-type $Hg_{0.8}Cd_{0.2}Te$ is more swollen compared to p-type material which is obvious because at the annealing process in the Hg-vapor atmosphere was introduced in the lattice of the n-type material, considerable number of the Hg-atoms – part of them filled the vacancies but another part left in the interstitial positions. While in case of the p-type material (as grown) there are huge number of the Hg-vacancies which result in contraction of the lattice. Therefore, the X-ray structural analyses confirmed our hypothesis that in the case of n-type material there are considerably fewer number

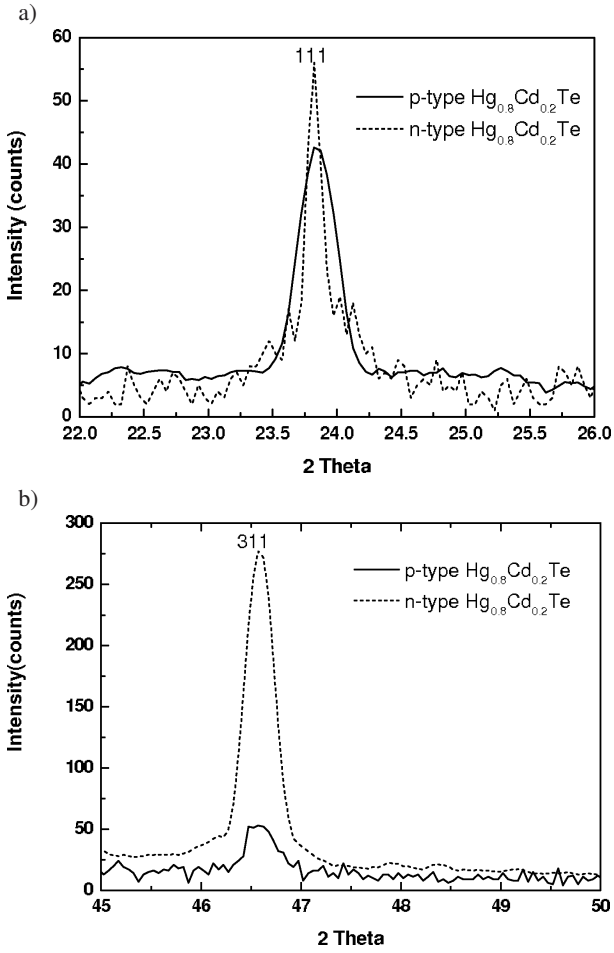

Fig. 12. Difraction X-ray spectra $Hg_{0.8}Cd_{0.2}Te$ at 300 K, a) comparison 111 peaks for n and p-type $Hg_{0.8}Cd_{0.2}Te$, b) comparison 311 peaks for n and p-type $Hg_{0.8}Cd_{0.2}Te$

of the Hg-vacancies than in the p-type material which is reflected both in the phonon spectra and in the X-ray diffraction spectra. It is not obvious for all n-$Hg_{0.8}Cd_{0.2}Te$ samples. In Fig. 12b is show the X-ray diffraction maximum for plane (311) which indicates the degree of the lattice ordering. In the case of the n-type $Hg_{0.8}Cd_{0.2}Te$ this maximum is many times sharper and higher than for p-type $Hg_{0.8}Cd_{0.2}Te$. It confirms our assumption about the comparably high quality of the crystal lattice for n-$Hg_{0.8}Cd_{0.2}Te$ though the level of the lattice defects it seems to be high too.

From X-ray measurement we may see that the lattice parameters are large for p-type $Hg_{0.8}Cd_{0.2}Te$ than for n-type $Hg_{0.8}Cd_{0.2}Te$.

8. General description of the phonon spectra in the HgCdTe alloys

If temperature increases, the number of Hg-atoms occupying the meta-stable positions (Hg^{II}) increases also and the deformation of the crystal lattice rises, respectively. The last factor should cause the removal of degeneracy of the HgTe-like CPMs in n-$Hg_{0.8}Cd_{0.2}Te$ when the temperature increases above 100 K (see Fig. 9): the APMs appear simultaneously, too. Indeed, the APM at 112 cm^{-1} (beside very weak from 30 K at 108 cm^{-1}) take place after 100 K in the n-type $Hg_{0.8}Cd_{0.2}Te$ and after 200 K, APM at 115–116 cm^{-1} appears. The presence of Hg^{II} in a tetrahedron leads to the stretching of bonds which in its turn causes the shift of the Hg-Te oscillation frequency towards smaller frequencies. This effect can occur in three kinds of tetrahedra: 1) containing 3 Hg-atoms in a stable position (Hg^{I}) and one Hg^{II}; 2) containing two Hg^{I}, one Cd-atom and one Hg^{II}; 3) containing one Hg^{I}, two Cd-atoms and one Hg^{II}. The frequencies of Hg-Te oscillations in these three type of tetrahedra should be arranged in the following sequence: the lowest frequency corresponds to the Hg-Te oscillations in the tetrahedron of the first type and highest corresponds to the oscillations in the tetrahedron of the third type.

The lines in the range of 135–137 cm^{-1} are generated as could be assumed, by the oscillation of the Cd-Te pair in the tetrahedra containing two Hg^{I}, one Cd-atom and one Hg^{II}.

9. Conclusions

The two-well model of the potential for Hg atoms in the $Hg_xCd_{1-x}Te$ crystal lattice was developed and confirmed by experimental results of FTIR and X-ray analysis. It was shown that the interpretation of the observed APM with the help of two-valley model is the most realistic hypothesis in comparison to the vacancy-model.

The temperature dependences of sums of the oscillator strengths for APM in the range 104–116 cm^{-1} for n- and the p-type CdHgTe shows the activation energy of 90 meV and 75 meV, respectively which corresponds to the transition energy of the mercury atoms from a deeper minimum to second (meta-stable) position.

The long-time annealing of HgCdTe at 220°C (inversion to the n-type) leads to the relaxation of lattice and return of Hg atoms to the stable state. The data of X-ray structure analyses confirms this hypothesis.

Reassuming, we can affirm that in the case of the p-type crystals the HgCdTe-lattice consists of two coexisting and penetrating sub-lattices:

The first sub-lattice contains the atoms of mercury in the stable state with the shorter length bonds of Hg-Te;

The second sub-lattice contains the Hg atoms in the meta-stable state with the longer bond of Hg-Te.

The phonon spectra of MCT are reproduced for each mentioned sub-lattices. An increase in temperature leads to the growth of the Hg-atom number in the meta-stable state and simultaneously to the enlargement of the Hg-Te bonds (tensions in the lattice) which leads to the frequency splitting of the HgTe-like CPMs in the n-type material. Due to this the differences between the phonon spectra of the n- and p-type HgCdTe disappears at the room temperature.

An increase of the content of CdTe in the HgCdTe crystal leads to the same effect as an increase of the temperature: results in the increase of the number of the CPMs (to the frequency splitting for both HgTe-like and CdTe-like modes). This takes place because the content of the mercury atoms in the meta-stable state increases and due to the enlargement of the Hg-Te bonds (increase tensions in the crystalline lattice) the degeneracy of the CPMs is removed

Acknowledgments. I would like to pass my thanks to Prof. E.M. Sheregii for his concept and helpfull discussion, dr J. Cebulski for KK transformation and A. Polit for X-ray measurements.

REFERENCES

[1] A. Rogalski, "HgCdTe infrared detector material: history, status and autlook", *Rep. Prog. Phys.* 68, 2267–2336 (2005).

[2] P. Martyniuk and A. Rogalski, "Quantum-dot infrared photodetectors. Status and autlook", *Prog. Quantum Electron.* 32, 89–120 (2008).

[3] P. Madejczyk, A. Piotrowski, K. Kłos, W. Gawron, A. Rogalski, J. Rutkowski, and W. Mróz, "Surface smoothness improvement of HgCdTe layers grown by MOCVD", *Bull. Pol. Ac.: Tech.* 57, 139–146 (2009).

[4] A. Piotrowski, P. Madejczyk, W. Gawron, K. Kłos, J. Pawluczyk, M. Grudzień, J. Piotrowski, and A. Rogalski, "Growth of MOCVD HgCdTe heterostructures for uncooled infrared photodetectors", *Bull. Pol. Ac.: Tech.* 53, 139–149 (2005).

[5] R.A. Mayanovich, W.F. Pong, and B.A. Bunker, "X-ray – absorption fine – structure studies of $Hg_{1-x}Cd_xTe$ and $Hg_{1-x}Mn_xTe$ bond lengths: bond relaxation and structural stability of ternary alloys", *Phys. Rev.* B 42, 11174–11182 (1990).

[6] A. Sher, A.B. Chen, W.E. Spicer, and K. Shih, "Effects influencing the structural integrity of semiconductors and their alloys", *J. Vac Sci. Technol.* A3, 105–111 (1985).

[7] D. Chandra, H.F. Schaake, J.H. Tregilgas, F. Aqariden, M.A. Kinch and A.J. Syllaios, "Vacancies in $Hg_{1-x}Cd_xTe$", *J. Electronics Materials* 29, 729–732 (2000).

[8] B.V. Robouch, A. Kisiel, E.M. Sheregii, "Temperature dependence discontinuity of the phonon mode frequencies caused by

a zero- gap state in HgCdTe alloys", *Phys. Rev.* B 64, 73204-1–73204-3 (2001).

[9] A.A. Maradudin, "Theoretical and experimental aspects of the defects and disorder on the vibrations in crystals", in: *Solid State Physics* vol. 18–19, ed. H. Ehrenreich, New York, 1966.

[10] S. Mitra, "Vibration spectra of solids", *Solid State Physics*, vol. 13, ed. H. Ehrenreich, New York, 1962.

[11] J. Polit, E.M. Sheregii, J. Cebulski, B.V. Robouch, A. Marchelli, M. Cestelli Guidi, M. Piccinini, A. Kisiel, P. Zajdel, E. Burattini, and A. Mycielski, "Phonon and vibrational spectra of hydrogenated CdTe", *J. Appl. Phys.* 100, 013521-1–013521-10 (2006).

[12] J. Polit, E.M. Sheregii, A. Kisiel, B.V. Robouch, A. Marcelli, and J. Cebulski, "Additional phonon modes and canonical phonon modes in CdHgTe", *Phys. Rev.* B 82, 014306-1–014306-12 (2010).

[13] A.S. Barker and J. Sievers, "Optical studies of the vibrational propertiesof disordered solids", *Rev. Modern Phys.* 47, S1–S179 (1975).

[14] R.C. Newman, "Local vibrational mode spectroscopy of defects in III/V compound", in: *Semiconductors and Semimetals*, vol. 38, pp. 117–187, Academic Press, New York, 1993.

[15] A.M. Kosevich, "The crystal lattice", *WILEY-VCH*, Berlin-New York, 1999.

[16] J. Cebulski, E.M. Sheregii, J. Polit, A. Marchelli, M. Piccinini, A. Kisiel, I.V. Kucherecho, and R. Triboulet, "Far – infrared reflectivity as a probe of point defects in Zn and Cd- doped HgTe", *Apll. Phys. Lett.* 92, 121904-1–1219904-3 (2008).

[17] S.P. Kozyrev, L.K. Vodopyanov, and R. Triboulet, "Structural analysis of the semiconductor – semimetals alloy $Cd_{1-x}Hg_xTe$ by infrared lattice – vibrational spectroscopy", *Phys. Rev.* B 58, 1374–1384 (1998).

[18] Li Biao, Y. Gui, Z. Chen, H. Ye, J. Chu, S. Wang, R. Ji, and L. He, "Study of impurity states in *p*-type $Hg_{1-x}Cd_xTe$ using far-infrared spectroscopy", *Appl. Phys. Lett.* 73, 1538–1540 (1998).

[19] J.H. Chu and S.C. Shen, "The study of far-infrared phonon spectra on $Hg_{1-x}Cd_xTe$", *Semicond. Sci. Technol.* S1, S86–S89 (1993).

[20] D.N. Talwar, "Vibrational properties of HgCdTe system", *J. Appl. Phys.* 56, 1601–1607 (1984).

[21] P.M. Amirtharaj, N.K. Dhart, J. Baars, and H. Seelewind, "Investigation of photons in HgCdTe using Raman Scattering and far-infrared reflectivity", *Semicond. Sci. Technol.* 5, S68–S72 (1990).

[22] S. Rath, K.P. Jain, S.C. Abbi, C. Julien, and M. Balkanski, "Composition and temperature – induced effects on the phonon spectra of narrow-band – gap $Hg_{1-x}Cd_xTe$", *Phys. Rev.* B 52, (24), 17172–17183 (1995).

[23] M. Grynberg, R. Le Toullec and M. Balkanski, *Phys. Rev.* B 9, 517–526 (1974).

[24] S.P. Kozyrev, "Projavlenie anomalnych svoistv reszetocznych kolebanii HgTe v splavach $Hg_{1-x}Z_xTe$ (Z=Cd.Mn,Zn)", *Fizyka Tverdogo Tela* 53, 153–163 (2011), (in Russian).

[25] O. Pages, J. Souhabi, A.V. Postnikov, and A. Chafi, "Percolation versus cluster models for multimode vibration spectra of mixed crystals: GaAsP as a case study", *Phys. Rev.* B 80, 035204-1–035204-12 (2009).

[26] J.A. Sussmann, "Quantum mechanical theory of barrier crossing by ions in solids", *J. Phys. Chem. Solids* 28, 1643–1648 (1967).

[27] E.M. Sheregii, Yu.O. Ugrin, D.D. Shuptar, and O.M. Lesko, "Magnetofononnyj rezonans na smeszannych opticzeskich modach w telluridach kadmija i rtuti", *JETP Lett.* 47, 711–716 (1988), (in Russian).

[28] E.M. Sheregii and Yu.O. Ugrin, "CdHgTe phonon-spectra research by means of magnetophonon resonance", *Sol. State Comm.* 83, 1043–1046 (1992).

[29] R. Ciach, M. Faryna, M. Kuźma, M. Pociask, and E.M. Sheregii, "Oscillations of the composition of HgCdTe solid solution after laser annealing, *J. Cryst. Growth* 161, 234–238 (1996).

[30] M. Cestelli Guidi, M. Piccinini, A. Marcelli, A. Nucara, P. Calvani, and E. Burattini, "Optical performances of SINBAD, the synchrotron infrared beamline of DAΦNE", *J. Optical Society of America* A22, 2810–2816 (2005).

[31] H.W. Verleur and A.S. Barker Jr, "Infrared lattice vibrations in $GaAs_yP_{1-y}$ alloys", *Phys. Rev.* 149, 715–729 (1966).

[32] R. Krause, A. Klimakow, F.M. Kiessling, A. Polity, P. Gille, and M. Schenk, "Study of Hg vacancies in (Hg,Cd)Te after THM growth and post – growth annealing by positron annihilation", *J. Cryst. Growth* 101, 512–517 (1990).